Bis-pseudorotaxane Formation of Perylene Bisimide-Linked [60]Fullerene Dumbbell-Like Molecules with [10]Cycloparaphenylene

Iris Solymosi[a]
Juan Sabin[b,c]
Harald Maid[a]
Lea Friedrich[a]
Edurne Nuin[d]
M. Eugenia Pérez-Ojeda[*a]
Andreas Hirsch[*a]

[a] Department of Chemistry and Pharmacy, Friedrich-Alexander-University Erlangen-Nuremberg, Nikolaus-Fiebiger-Straße 10, 91058 Erlangen, Germany
[b] AFFINImeter-Software 4 Science Developments, S. L. Edificio Emprendia s/n Campus Vida, Santiago de Compostela, Spain
[c] Biophysics & Interfaces Group, Applied Physics Department, Facultade de Física, Universidade de Santiago de Compostela, 15782 Santiago de Compostela, Spain
[d] Instituto de Ciencia Molecular (ICMol), Universidad de Valencia, Catedrático José Beltrán 2, Paterna 46980, Spain
[*] eugenia.perez-ojeda@fau.de; andreas.hirsch@fau.de

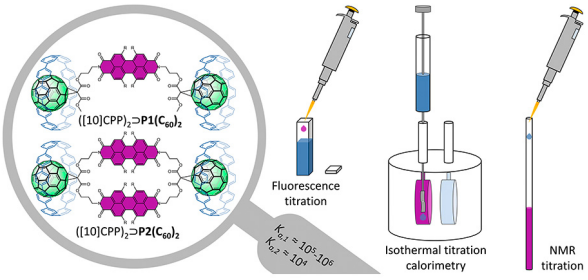

Received: 14.06.2022
Accepted after revision: 20.07.2022
DOI: 10.1055/a-1906-6875; Art ID: OM-2022-06-0008-OA

Abstract Two [60]fullerene dumbbell-like molecules with a single or double perylene-3,4,9,10-tetracarboxylic acid bisimide (PBI) linker were synthesized to study the structural and photophysical properties in addition to the complex formation with [10]cycloparaphenylene ([10]CPP). Due to their special optical properties, it is possible to describe the complexation using conventional spectroscopic methods such as NMR and fluorescence. However, isothermal titration calorimetry (ITC) was used to complete the analysis of the bis-pseudorotaxane formation by investigating the binding stoichiometries as well as the thermodynamic and kinetic parameters. It was observed that the PBI bridges do not inhibit the complexation with [10]CPP, giving rise to the formation of 1 : 1 and 1 : 2 complexes in *o*-dichlorobenzene with affinities of around $10^5 \cdot M^{-1}$, similar to the [10]CPP⊃C_{60} reference system. A novel global analysis by combination of data sets from different techniques allowed us to follow the species distribution very precisely. ITC has proven to be a very powerful method for studying the complexation between fullerene derivatives and strained carbon nanohoops, which provides not only binding affinities and stoichiometries, but also all thermodynamic and kinetic parameters of the bis-pseudorotaxane formation. These results are of significant interest for the investigation of fullerene complexes in supramolecular chemistry and for their future applications in semiconductors and optoelectronics.

Key words: supramolecular chemistry, host–guest systems, fullerenes, perylene bisimide, macrocycles, cyclophanes, carbon nanobelts

Introduction

Supramolecular chemistry has gained increasing interest in the last few decades because of its important role in many different fields like drug delivery, catalysis and sensing. An important part of supramolecular chemistry is host–guest recognition, in which the interplay of molecular sizes, complementary shapes, charge distribution as well as binding sites is of great importance.[1] In this sense, macrocyclic systems such as crown ethers,[2] calixarenes,[3] cyclodextrins,[4] and cycloparaphenylenes (CPPs)[5] are well suited as host molecules due to their molecular geometries. It is worth noticing that in CPPs, p-conjugated phenylene units are linked to each other resulting in hoop-shaped hosts suitable for complexing molecules with convex surfaces such as fullerenes. This shape complementarity is crucial for studying concave–convex as well as donor–acceptor interactions of these systems.[6] Iwamoto et al reported the first host–guest complex consisting of C_{60} and [10]CPP, where the complexation is due to an ideal size ratio of the two molecules involved.[7] Since then, further complexes of monomeric molecules such as C_{70} and [11]CPP[8] or $Li^+@C_{60}$ and [10]CPP[9] have been detected. Furthermore, examples of complexed dimeric molecules were examined as well, such as the 2 : 1 host–guest complex of [10]CPP and the dumbbell-shaped bis(azafullerene) $(C_{59}N)_2$,[10] a porphyrin [10]CPP conjugate and $(C_{60})_2$ dimer[11] or between C_{60} and a dimeric CPP with a rigid linker.[12] These supramolecular complexes could be also classified as pseudorotaxanes[13] like von Delius and co-workers

named their complex of a fullerene dimer and [10]CPP.[14] The corresponding host–guest interactions have been investigated theoretically[15] and experimentally using various spectroscopic methods, such as fluorescence,[6–7,10] UV-vis[7–9] or NMR[16]. All these methods rely on the indirect observation of a property variation upon complexation. Isothermal titration calorimetry (ITC) offers the advantage of quantifying the association constant, stoichiometry, thermodynamic parameters such as the changes of enthalpy, entropy and Gibbs free energy as well as kinetic parameters directly by measuring the heat of the interaction in a single experiment.[17] However, no literature report on the interaction between [10]CPP and C_{60} or other fullerene systems studied using ITC has appeared yet, which is why a detailed understanding of the thermodynamics and kinetics of the complexes and pseudorotaxane formation becomes an important issue. With this background, the goal of the present work is to determine binding stoichiometries and affinities as well as thermodynamic and kinetic parameters of three different fullerene guest molecules which form complexes with [10]CPP including C_{60} as a reference system using physical techniques such as ITC.

Specifically, motivated by the increasing interest of fullerene complexes as well as perylene bisimide (PBI) derivatives for application in optoelectronics[18] and semiconductors,[19] we decided to investigate systems bearing both components with special chiroptical and electrochemical properties to study the influence of the binding on the chiroptical properties. In addition, hybrid PBI cyclophanes functionalized with fullerenes have been chosen because they represent promising supramolecular hosts due the tunable electronic interactions between the PBI units,[20] the fluorescence sensing properties[20] and the modulation of the interaction by modification of the surrounding environment through hydrophobic or hydrophilic fullerenes.[21] Thus, two [60]fullerene dumbbell-like systems **P1(C$_{60}$)$_2$** and **P2(C$_{60}$)$_2$** were synthesized, in which the fullerene units are linked together via a single (**P1**) or double (**P2**) PBI bridge similar to that previously described by our group for hybrid PBI cyclophanes and linear systems with fullerene pentakisadducts.[21a] In addition, these particular systems allow evaluating the influence of the different bridging geometries in the complexation. Furthermore, due to their optical properties, it is possible to use different spectroscopic techniques such as fluorescence and NMR not only to investigate the binding affinity but also to understand their relative orientation and intramolecular atropisomer assembly in solution. For the first time, a multi-technique global analysis was performed using information from both spectroscopic and calorimetric techniques, which unambiguously reveals the thermodynamic parameters of the bis-pseudorotaxane formation as an enthalpically driven process.

Results and Discussion

The synthesis of the targeted dumbbell molecule **P1(C$_{60}$)$_2$** and macrocycle **P2(C$_{60}$)$_2$** was carried out using modified *Bingel–Hirsch* conditions with iodine as the halogenating agent starting from precursors **P1** and **P2**, which were prepared in a multi-step synthesis according to literature procedures (Scheme 1).[21a,22] Using these conditions, **P1(C$_{60}$)$_2$** was obtained in 51% yield. In addition to the cyclopropanation product, an isomeric mixture of the intramolecular fullerene bisadduct was formed in 33% yield. In order to avoid polymer formation and to obtain the highest possible yield of **P2(C$_{60}$)$_2$**, twice as many equivalents of C_{60} and double dilution were used compared to the synthesis of **P1(C$_{60}$)$_2$**. In addition, the Schwesinger phosphazene base P_1-*t*Bu was used instead of 1,8-diazabicycloundec-7-ene (DBU), due to the sterically more demanding **P2** precursor, which provided **P2(C$_{60}$)$_2$** in 45% yield. The target compounds were characterized by HRMS, HPLC, NMR (^{1}H and ^{13}C) as well as UV-vis and fluorescence spectroscopies.

The introduction of the fullerene substituents influences the optical properties of the hybrid systems as noticed by the comparison to the corresponding precursors.

The introduction of bulky aryloxy groups attached to the bay positions of PBI derivatives is a widespread approach to obtain soluble aromatic systems based on the distortion of their planarity. As expected, the *tert*-butylphenoxy substituents cause a twist of the PBI core leading to two different chiral orientations (*M*/*P*). Thus, the corresponding homochiral racemic mixture (*M*,*M*)-**P2(C$_{60}$)$_2$**/(*P*,*P*)-**P2(C$_{60}$)$_2$** and mesocate (*M*,*P*)-**P2(C$_{60}$)$_2$**/(*P*,*M*)-**P2(C$_{60}$)$_2$** are formed in the cyclophane structure. The UV-vis and fluorescence spectra of **P1** and **P2** as well as the targeted dumbbell molecules **P1(C$_{60}$)$_2$** and **P2(C$_{60}$)$_2$** in *o*-dichlorobenzene (*o*-DCB) measured at room temperature are presented in Figure 1.

The UV-vis absorption spectrum of **P1(C$_{60}$)$_2$** exhibits the same absorption features as **P1** with no evidence of π–π stacking in the characteristic S_0–S_1 PBI region from the 500 to 600 nm range. The main absorption bands displayed by the spectra exhibited absorption maxima at 546 and 588 nm, which belong to the 0–*1 and 0–*0 vibrational transitions. The ratio of these two transitions is 0.64 : 1, which allowed the quantification of the π–π stacking between the PBI units, with a stacking becoming stronger as the intensity of the 0–*1 transition increases.[23] In addition, a slight co-facial π–π stacking was found for **P2** dissolved in *o*-DCB with a ratio of 0.83 : 1, although this effect is not as prominent as in other non-halogenated solvents like THF or toluene.[21a] When comparing the absorption spectra of **P2** and **P2(C$_{60}$)$_2$**, the stacking is more pronounced for **P2(C$_{60}$)$_2$**, as indicated by the 0.95 : 1 ratio of the 0–*1 and 0–*0 intensities. This stacking has no further consequence in the absorption, since **P2** and **P2(C$_{60}$)$_2$**, each with two PBI moieties, show approximately twice the absorption coefficient as

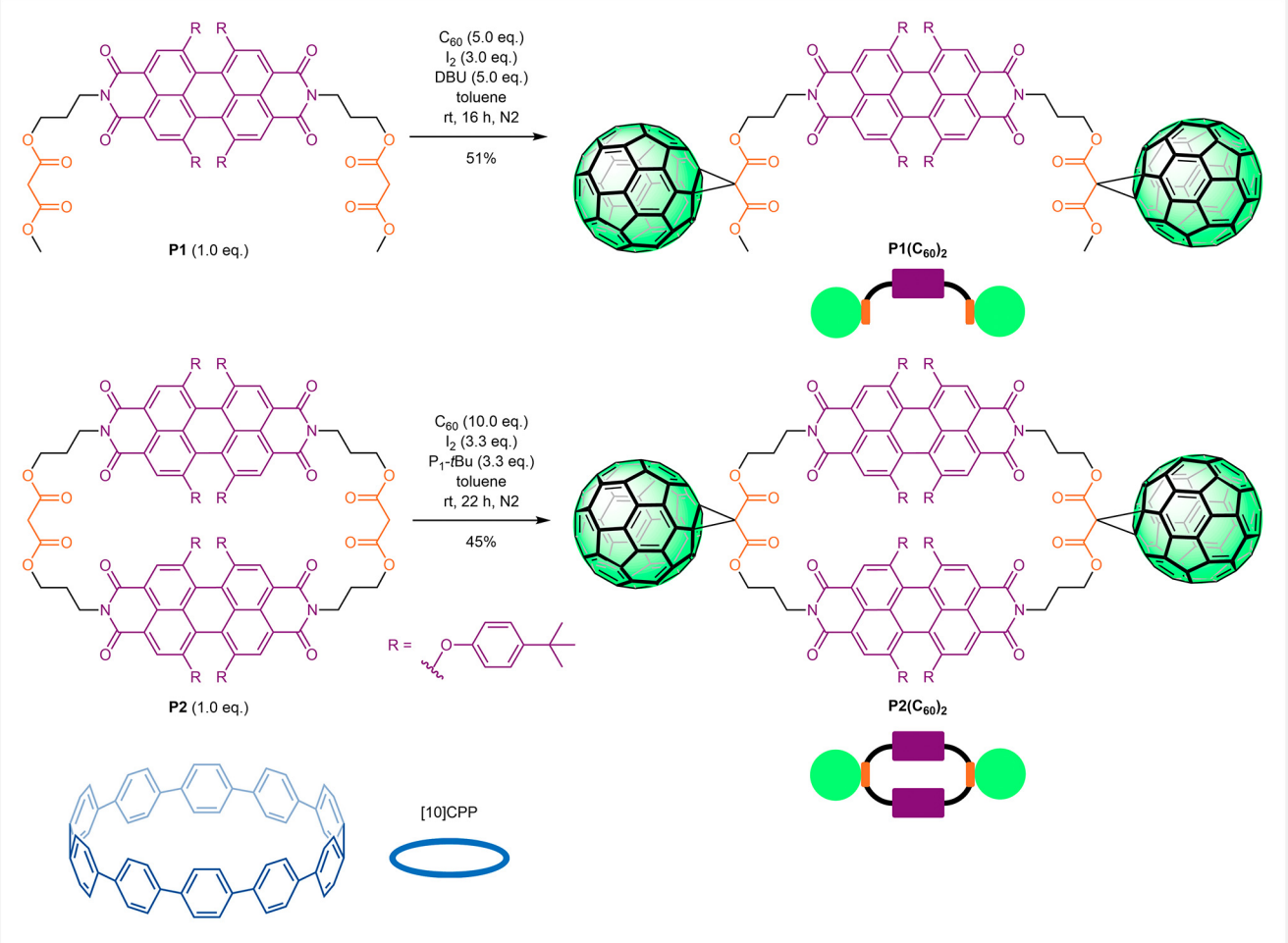

Scheme 1 Synthesis of the [60]fullerene dumbbell-like molecules **P1**(C_{60})$_2$ and **P2**(C_{60})$_2$ via the *Bingel–Hirsch* reaction and structure of [10]CPP together with their corresponding schematic representations.

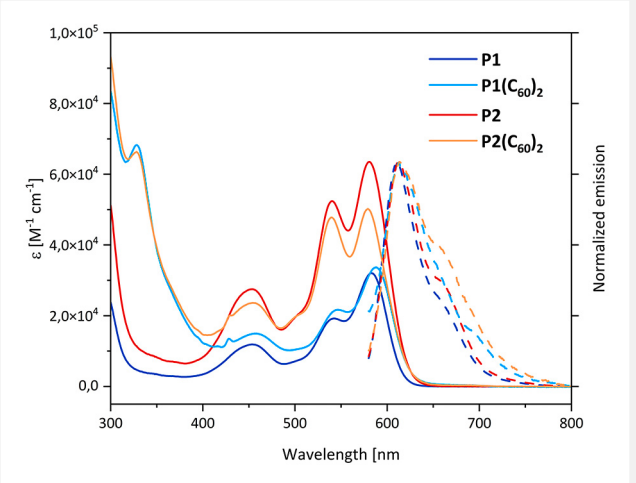

Figure 1 Absorption and normalized fluorescence spectra of the precursor molecules **P1** and **P2** as well as the hybrid systems **P1**(C_{60})$_2$ and **P2**(C_{60})$_2$ recorded in *o*-DCB at room temperature.

compared to **P1** and **P1**(C_{60})$_2$, which have only one PBI unit. However, due to the fullerene substituents, the absorption is increased at wavelengths below 500 nm[24] with a local maximum at 458 nm, corresponding to the S_0–S_2 transition.

The fluorescence emission spectra revealed a mirror-like image of the absorption spectra with a Stokes shift of 27, 25, 32 and 24 nm for **P1, P1**(C_{60})$_2$, **P2** and **P2**(C_{60})$_2$, respectively, and the fluorescence maximum of **P1** at 610 nm is slightly blue-shifted in comparison to the other three molecules with a maximum at 613 nm. The fluorescence shoulder of **P2** at around 660 nm evolved into an even more intense one for **P2**(C_{60})$_2$, indicating aggregation which is in agreement with the ratio of the 0–*1 and 0–*0 absorption intensities.[25] It is noteworthy to mention that **P1**(C_{60})$_2$ exhibits an additional shoulder at around 700 nm that can be assigned to the methanofullerene substituents.[24]

At this point, we decided to examine the diastereomeric composition of (*M*,*M*)-**P2**(C_{60})$_2$/(*P*,*P*)-**P2**(C_{60})$_2$ and (*M*,*P*)-**P2**(C_{60})$_2$/(*P*,*M*)-**P2**(C_{60})$_2$. For this purpose, tempera-

ture-dependent NMR experiments were carried out. The relatively strong co-facial π–π stacking of **P2(C$_{60}$)$_2$** is also apparent in the temperature-dependent NMR investigations shown in Figure 2. The spectra were recorded in 1,1,2,2-tetrachloroethane for better comparability with our previous investigations, which will be discussed later. As previously mentioned, the *tert*-butylphenoxy substituents at the bay positions are responsible for the PBI twisted core and the differentiation into two different atropisomers (*M*/*P*). For **P2(C$_{60}$)$_2$** the signals at room temperature are greatly broadened and split compared to the spectrum at higher temperatures. This indicates that atropisomerization is slow at the NMR timescale. Because **P2(C$_{60}$)$_2$** occurs as a racemic mixture of two diastereoisomers, we see split signals that become sharper upon cooling. The main signals can be assigned to the racemic mixture of the homochiral (*M*,*M*)-**P2(C$_{60}$)$_2$**/(*P*,*P*)-**P2(C$_{60}$)$_2$** (see Figure 2, a–g), where the π–π interactions are stronger due to the homochiral arrangement and shorter distances between the PBI units. In contrast, the less intense signals belong to the mesocate (*M*,*P*)-**P2(C$_{60}$)$_2$**/(*P*,*M*)-**P2(C$_{60}$)$_2$** (see Figure 2, a′).[21a] The integral ratio between (*M*,*M*)-**P2(C$_{60}$)$_2$**/(*P*,*P*)-**P2(C$_{60}$)$_2$** and (*M*,*P*)-**P2(C$_{60}$)$_2$**/(*P*,*M*)-**P2(C$_{60}$)$_2$** is approximately 5 : 1 at −15 °C dissolved in $C_2D_2Cl_4$ (see Figure S1 in the Supporting Information), for the precursor molecule **P2** the ratio of (*M*,*M*)-**P2**/(*P*,*P*)-**P2** and (*M*,*P*)-**P2**/(*P*,*M*)-**P2**, is 10 : 1. Our previous work has also described the synthesis of fullerene hybrids where the fullerenes were fivefold-functionalized via the *Bingel–Hirsch* cyclopropanation with diethyl malonates named as **P2F2$_{Et}$** and in the case of this ethyl-functionalized hybrid, exclusively (*M*,*M*)-**P2F2$_{Et}$**/(*P*,*P*)-**P2F2$_{Et}$** could be detected.[21a] It is thus interesting to note that the substitution with fullerenes alone does not increase the diastereoselectivity, but in fact reduces it, and that it is only improved by the additional functionalization of the fullerenes.

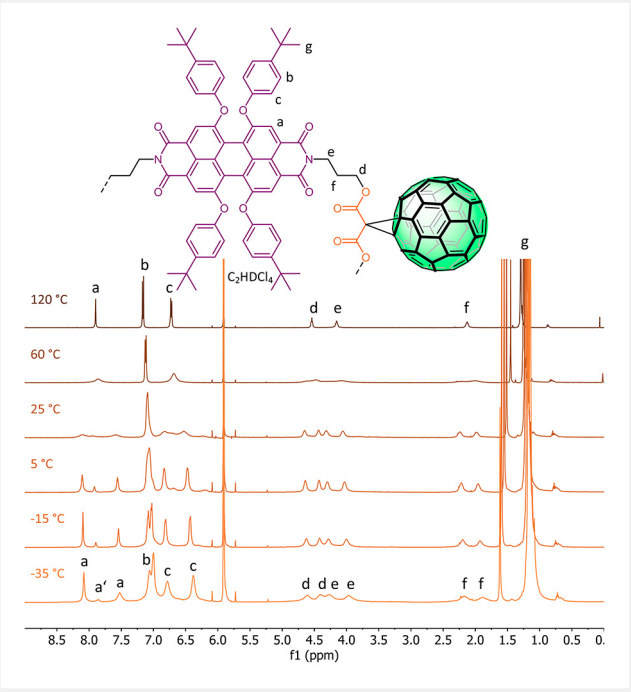

Figure 2 Temperature-dependent ^{1}H NMR (500 MHz) spectra of **P2(C$_{60}$)$_2$** recorded in $C_2D_2Cl_4$.

Upon heating, each set of signals coalesces so that at 120 °C only a single set of sharp signals is observed. The coalescence temperatures for **P2(C$_{60}$)$_2$** are intermediate between those of **P2** and **P2F2$_{Et}$**,[21a] indicating that the inversion barrier is larger than that for **P2** but smaller compared to **P2F2$_{Et}$**. This could be confirmed by calculating the activation energy $\Delta G^{\ddagger}$ for the conformational interconversion of the diastereoisomers using the coalescence method (see Equation 1 in the Supporting Information).[26] The activation energy in $C_2D_2Cl_4$ for **P2(C$_{60}$)$_2$** ($\Delta G^{\ddagger} = 60.1\ kJ \cdot mol^{-1}$) lies between the values of **P2** ($\Delta G^{\ddagger} = 57.0\ kJ \cdot mol^{-1}$) and **P2F2$_{Et}$** ($\Delta G^{\ddagger} = 64.0\ kJ \cdot mol^{-1}$).[21a] This can be explained by the fact that **P2(C$_{60}$)$_2$** is more sterically hindered than **P2** because of the fullerene substituents, but less hindered compared to **P2F2$_{Et}$**, which has additional ethyl side chains on the fullerenes. In contrast, the initially mentioned atropisomerization of the *M* and *P* isomers is fast on the NMR timescale for **P1(C$_{60}$)$_2$**, which is why one set of sharp signals could be already seen at room temperature.

Starting from the dumbbell-like molecules **P1(C$_{60}$)$_2$** and **P2(C$_{60}$)$_2$**, the corresponding pseudorotaxanes with [10]CPP were investigated by spectroscopic as well as calorimetric techniques. The host–guest complex [10]CPP⊃C_{60} serves as a reference system for the later investigations of the hybrid systems and has already been examined by means of fluorescence titration in toluene[6–7] and UV-vis titration in *o*-DCB.[7] We have characterized it for the first time with ITC. Triple titration calorimetric experiments were performed to afford the association constant of $K_a = (2.5 \pm 0.1) \cdot 10^5 \cdot M^{-1}$ and a 1 : 1 complex using the stoichiometric approach for [10]CPP⊃C_{60} in *o*-DCB. An enthalpy-driven complexation was revealed with the thermodynamic parameters of $\Delta H = -6.08\ kcal \cdot mol^{-1}$, $\Delta G = -7.35\ kcal \cdot mol^{-1}$ and $\Delta S = 4.26\ cal\ mol^{-1} \cdot K^{-1}$ (see Figure S4 in the Supporting Information). The binding constant is 2 orders of magnitude higher than the value reported in the literature[7] $K_a = (6.0 \pm 0.2) \cdot 10^3 \cdot M^{-1}$ obtained by UV-vis titration (see Table 1).

Given this discrepancy, an additional triple fluorescence titration was performed in order to corroborate our result, which yielded the same order of magnitude as our ITC experiments with a binding constant of $K_a = (8.09 \pm 0.02) \cdot 10^5 \cdot M^{-1}$ (see Table 1 and Figure S9 in the Supporting Information). The binding constant obtained by fluorescence titration is a bit overestimated in comparison to that obtained by the ITC titration due to the inner filter effect consequence of a certain overlap of the absorption bands.[27] To verify that our fluorescence titration in *o*-DCB is trustworthy, we re-

Table 1 Comparison of different comparable host–guest systems reported in the literature and this work.

System	Titration method	Solvent	Binding constant K_a [M^{-1}]	Ref.
[10]CPP⊃C_{60}	Fluores.	Tol	$(2.79 \pm 0.03) \cdot 10^6$	7
[10]CPP⊃C_{60}	Fluores.	Tol	$3.6 \cdot 10^6$	6
[10]CPP⊃C_{60}	Fluores.	Tol	$(8.40 \pm 0.03) \cdot 10^6$	
[10]CPP⊃C_{60}	UV/vis	*o*-DCB	$(6.0 \pm 0.2) \cdot 10^3$	7
[10]CPP⊃C_{60}	ITC	*o*-DCB	$(2.5 \pm 0.1) \cdot 10^5$	
[10]CPP⊃C_{60}	Fluores.	*o*-DCB	$(8.09 \pm 0.02) \cdot 10^5$	
$([10]CPP)_2$⊃$(C_{59}N)_2$	Fluores.	Tol	$K_1 = 8.4 \cdot 10^6$ $K_2 = 3.0 \cdot 10^6$	10
$(C_{60})_2$⊃[10]CPP dimer	UV/vis	*o*-DCB	$K_1 = (4.15 \pm 0.58) \cdot 10^5$ $K_2 = (3.63 \pm 0.44) \cdot 10^3$	12
C_{60}⊃porphyrin [10]CPP conjugate	Fluores.	Tol	$(1.6 \pm 0.1) \cdot 10^6$	11
PCBM⊃porphyrin [10]CPP conjugate	Fluores.	Tol	$(3.7 \pm 0.1) \cdot 10^5$	11
$(PCBM)_2$⊃[10]CPP dimer	UV/Vis	CH_2Cl_2	$K_1 = (7.46 \pm 0.33) \cdot 10^5$ $K_2 = (5.85 \pm 0.25) \cdot 10^4$	28
Fullerene rotaxane⊃[10]CPP dimer[a]	Fluores.	Tol	$1.1 \cdot 10^6$	14

[a]Only the binding constant according to the evaluation with a 1 : 1 binding model is given.

produced the fluorescence titration of Yamago and co-workers in toluene[7] (see Table 1), obtaining a similar binding constant of $K_a = (8.40 \pm 0.03) \cdot 10^6 \cdot M^{-1}$ compared to $(2.79 \pm 0.03) \cdot 10^6 \cdot M^{-1}$ described above[7] (see Table 1 and Figure S10 in the Supporting Information). This result is also in agreement with other fullerene derivatives[10–11,14] and CPP conjugates[11–12,28], which exhibit affinities in the range of 10^5–$10^6 \cdot M^{-1}$ (see Table 1). The order of magnitude difference of our binding constants in toluene and *o*-DCB can be explained by the fact that C_{60} is better soluble in *o*-DCB than in toluene.

Furthermore, our values in *o*-DCB obtained by ITC and fluorescence titrations are very well comparable to the first binding constant of the $(C_{60})_2$⊃[10]CPP dimer complex, in which the binding constant in *o*-DCB is of the same order of magnitude (see Table 1).[12]

Subsequently, the complexation of functional dumbbells with [10]CPP was examined using different techniques (fluorescence, ITC and NMR). In order to fully understand the different stoichiometries of the system, two kinds of titrations, shown in Figure 3, were performed. One of them was carried out with a constant [10]CPP concentration and an increasing concentration of **P1(C_{60})$_2$** (Exp. A), whereas in the other titration the concentration of [10]CPP was increased while keeping constant the concentration of **P1(C_{60})$_2$** (Exp. B).

We started with absorption and fluorescence investigations of the complexation of **P1(C_{60})$_2$** and [10]CPP. It could

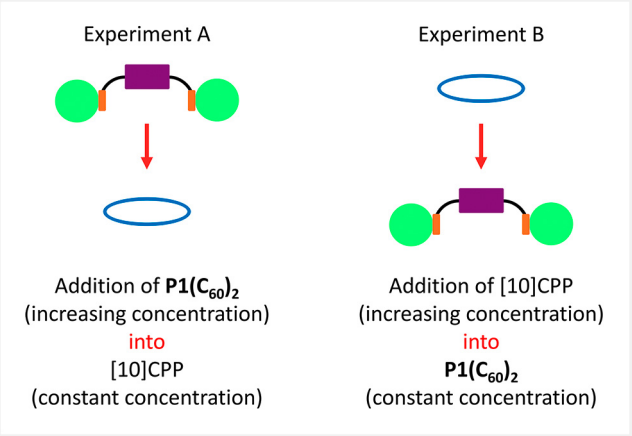

Figure 3 Schematic representation of the two different titration experiments A and B that are feasible with ITC.

be shown that the absorption or fluorescence behavior of the PBI unit is not influenced by the addition of [10]CPP (see Figures S14 and S11 in the Supporting Information).

However, similar to the addition of C_{60}, the [10]CPP fluorescence is quenched upon addition of the dumbbell-like molecule, which can be seen in Figure 4b. This procedure corresponds to Exp. A (see Figure 3), with different equilibria and complexes being conceivable (see Figure 4a). Therefore, the fluorescence titration data were analyzed with different binding models. The 1 : 1 binding model yields a binding constant of $K_a = (3.55 \pm 0.02) \cdot 10^5 \cdot M^{-1}$ with a relatively small standard deviation (see Figure S12a in the Supporting Information). However, other binding models such as 2 : 1 and 1 : 2 fit the experimental data fairly well. The sequential 2 : 1 model, with two [10]CPPs binding to one **P1(C_{60})$_2$**, provides the best fitting with stoichiometry binding constants of $K_{a,1} = (7.2 \pm 0.1) \cdot 10^5 \cdot M^{-1}$ and $K_{a,2} = (7.9 \pm 0.9) \cdot 10^5 \cdot M^{-1}$ (see Figure 4c,d). All the performed analyses reveal that 1 : 1 complexes are predominant during the titration. This is the reason why adding a second reaction, either 2 : 1 or 1 : 2, has little effect on the fitting (see Figure S12c in the Supporting Information).

In order to get a clear conclusion about the stoichiometry, a titration experiment where [10]CPP is in excess is needed. Since we cannot use fluorescence measurements to perform the inverse experiment (Exp. B) and saturate the hybrid system with an excess of [10]CPP due to absorption band overlap, we investigated the binding behavior with ITC to also obtain the thermodynamic parameters and the stoichiometry. ITC offers the advantage of carrying out the titration in both directions. On the one hand, the titration can be done as already investigated by fluorescence, where the hybrid is added to the [10]CPP (Exp. A); on the other hand, it is also possible to have an increasing concentration of [10]CPP by reversing the titration and adding [10]CPP to the hybrid (Exp. B). A global analysis of the triplicate titration of

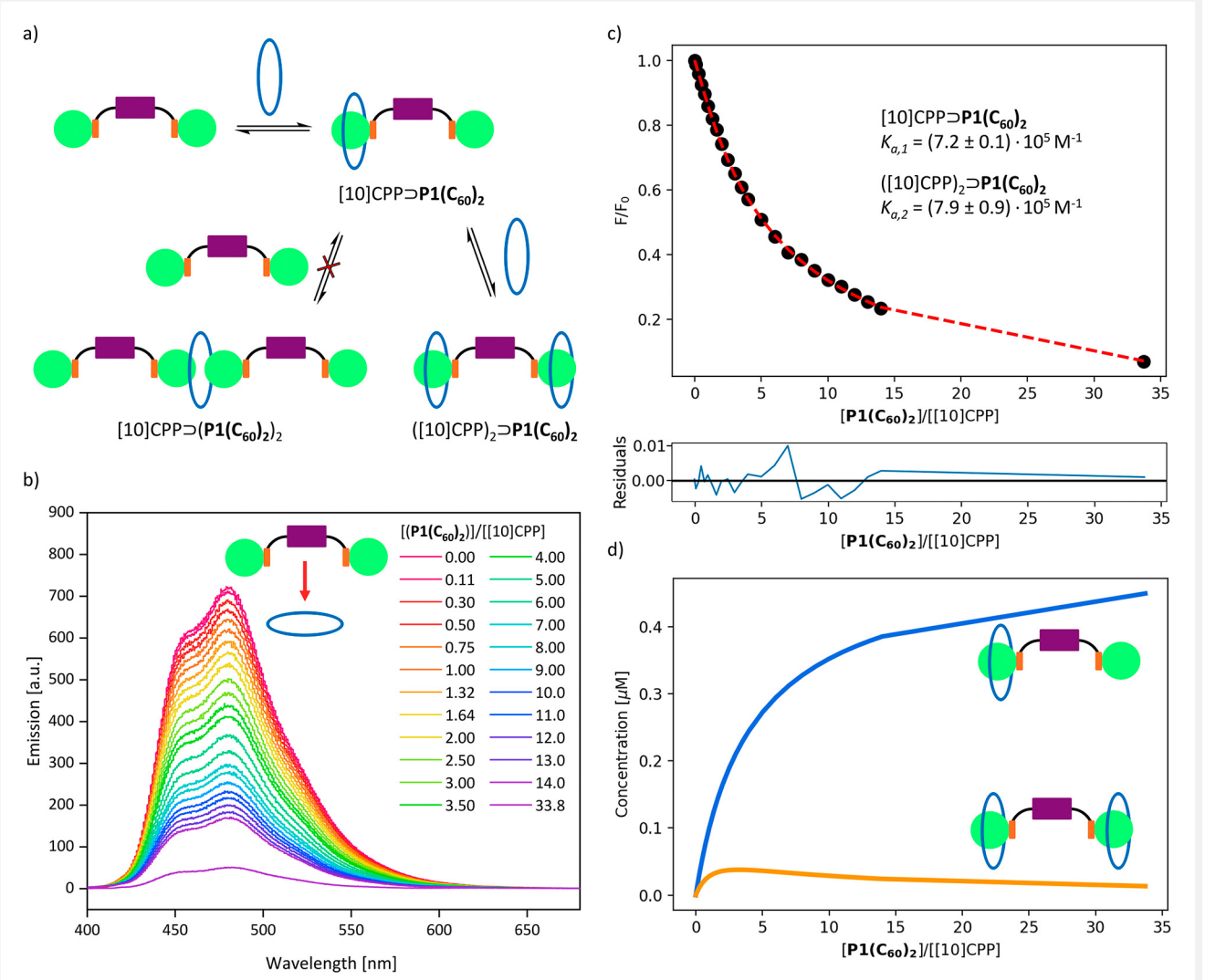

Figure 4 a) Schematic representation of the different possible complexes out of **P1(C$_{60}$)$_2$** and [10]CPP in Exp. A. b) Fluorescence spectra (λ = 370 nm) of **P1(C$_{60}$)$_2$** (c = 0.0–1.73 · 10^{-5} mol · L^{-1}) into [10]CPP (c = 5.13 · 10^{-7} mol · L^{-1}) in *o*-DCB. c) Fitting (red line) of the experimental data (black points) with a 2 : 1 binding model leading to the two binding constants $K_{a,1}$ and $K_{a,2}$ as well as residuals of the fit with respect to the experimental data (blue line). d) Species evolution of [10]CPP⊃**P1(C$_{60}$)$_2$** (blue) and ([10]CPP)$_2$⊃**P1(C$_{60}$)$_2$** (orange) during the titration.

P1(C$_{60}$)$_2$ over [10]CPP (Exp. A) with the independent sites binding model gave a stoichiometry value of n = 0.741 and a binding constant of K_a = (2.5 ± 0.4) · 10^5 · M^{-1} (see Table 2 and Figure S5 in the Supporting Information). Thus, the stoichiometry is necessarily a mixture of species, namely, the 2 : 1 complex ([10]CPP)$_2$⊃**P1(C$_{60}$)$_2$** (n = 0.5) and the 1 : 1 complex [10]CPP⊃**P1(C$_{60}$)$_2$** (n = 1.0). Consequently, the results of the ITC are in perfect agreement with the fittings of the fluorescence titration. Furthermore, we assume that the solvent affects not only the binding constants, but also the stoichiometry. Wegner et al[10] have already shown in their investigations of (C$_{59}$N)$_2$ and [10]CPP that simply by changing the solvent from toluene to *o*-DCB, the maximum of the Job's plot is shifted from 0.3 to 0.4, demonstrating a different stoichiometry of the complex formed. It is therefore possible that in our case the solvent also contributes to the stoichiometry of 0.741 involving a mixture of species. Moreover, it is important to consider that Job's plots have limited applicability in studying host–guest supramolecular interactions; they can be misleading and require a very careful experiment execution and interpretation. For this reason, the direct evaluation of the stoichiometry by ITC is a reliable result and a great advantage over the previously used methods.

It seems counterintuitive that the 2 : 1 complex ([10]CPP)$_2$⊃**P1(C$_{60}$)$_2$** can be formed despite the excess of **P1(C$_{60}$)$_2$**. Therefore, the inverse titration (Exp. B) was per-

Table 2 Summary of the different analyses of the ITC titrations giving the binding affinities as well as stoichiometric and thermodynamic parameters.

Syringe (A) into Cell (M)	Model	n^a	K_a [M^{-1}]	ΔH [kcal·mol^{-1}]	ΔG [kcal·mol^{-1}]	ΔS [cal·mol^{-1}·K^{-1}]
P1(C$_{60}$)$_2$ into [10]CPP	Independent sites	0.748	$(2.5 \pm 0.4) \cdot 10^5$	-8 ± 1	−7.37	−2.59
[10]CPP into **P1(C$_{60}$)$_2$**	Independent sites	1.908	$(4.1 \pm 0.2) \cdot 10^5$	-4.50 ± 0.07	−7.65	8.92
P1(C$_{60}$)$_2$ into [10]CPP (Exp. A) and inverse (Exp. B)	Stoichiometric equilibria: Global analysis with 2 : 1 and 1 : 2	/	$K_1 = (9.2 \pm 0.2) \cdot 10^5$ $K_2 = (8.9 \pm 0.2) \cdot 10^4$	$\Delta H_1 = -5.88 \pm 0.01$ $\Delta H_2 = -5.93 \pm 0.01$	$\Delta G_1 = -8.13$ $\Delta G_2 = -6.75$	$\Delta S_1 = 7.55$ $\Delta S_2 = 2.76$
P2(C$_{60}$)$_2$ into [10]CPP (Exp. A) and inverse (Exp. B)	Stoichiometric equilibria: Global analysis with 2 : 1 and 1 : 2	/	$K_1 = (1.07 \pm 0.02) \cdot 10^6$ $K_2 = (6.2 \pm 0.2) \cdot 10^4$	$\Delta H_1 = -5.32 \pm 0.01$ $\Delta H_2 = -4.89 \pm 0.01$	$\Delta G_1 = -8.22$ $\Delta G_2 = -6.53$	$\Delta S_1 = 9.73$ $\Delta S_2 = 5.51$

[a]When using the independent sites model it is considered that all sites are independent. This model provides a reaction scheme where the host with a certain number of sites "*n*" binds to the guest. We use the independent sites model first to establish the stoichiometry so that we can select the appropriate binding model (2 : 1 or 1 : 2) in the following step for the global analysis with the stoichiometric equilibria approach. When using the stoichiometric equilibria model the stoichiometry is fixed by the selected binding model (2 : 1 or 1 : 2), which is why there is no value for *n* given.

formed with an excess of [10]CPP in order to saturate the system and corroborate the formation of the bis-pseudorotaxane. In the global analysis of the triple titration with the independent model, a stoichiometry of $n = 1.908$ and a binding affinity of $K_a = (4.1 \pm 0.2) \cdot 10^5 \cdot M^{-1}$ were achieved (see Table 2 and Figure S6 in the Supporting Information). The stoichiometry is almost 2, confirming the formation of ([10]CPP)$_2$⊃**P1(C$_{60}$)$_2$**. Subsequently, it was possible to fit all six ITC isotherms of both titration series in a global analysis using the stoichiometric equilibria approach in order to better understand the species distribution.[29]

The triplicates of direct and reverse experiments (Exp. A and B in Figure 3) were fitted using the same binding model and the same thermodynamic parameter (binding constant and enthalpy). The parameters obtained from this global analysis are summarized in Table 2 and the species distributions are shown in Figure 5. It can be clearly seen that in the titrations, where **P1(C$_{60}$)$_2$** was added (Exp. A) (Figure 5c), the 1 : 1 complex [10]CPP⊃**P1(C$_{60}$)$_2$** is mainly present at the end of the titration, whereas by adding [10]CPP (Exp. B), the 1 : 2 complex ([10]CPP)$_2$⊃**P1(C$_{60}$)$_2$** is predominantly seen at the end of the titration (Figure 5f). The binding constant for the 1 : 1 complex is $K_{a,1} = (9.2 \pm 0.2) \cdot 10^5 \cdot M^{-1}$ and for the 1 : 2 complex $K_{a,2} = (8.9 \pm 0.2) \cdot 10^4 \cdot M^{-1}$.

Interestingly, the broadening of the peaks during the ITC titration can give information about the binding kinetics.[30] The equilibration time curve shown in Figure 6 represents the time required for the signal to come back to the baseline for each titration as a function of concentration ratio for direct and reverse ITC experiments. This clearly shows a maximum near the saturation of the system when the concentration of free species is lowest and the interaction becomes slower. "kinITC" is the method implemented in AFFINImeter to obtain k_{on} and k_{off} values out of the equilibration time curve.[31] Despite this method can only be applied for a 1 : 1 interaction, we consider that this is still a good approximation to estimate the kinetics of our system at concentration ratios where the 1 : 1 complex is predominant (according to the species distribution plot of Figure 5c and 5f). Both equilibration time curves can be fitted with $k_{on} = (4 \pm 1) \cdot 10^3 \cdot M^{-1} \cdot s^{-1}$ and $k_{off} = (1.1 \pm 0.2) \cdot 10^{-2} \cdot s^{-1}$.

The response time of the calorimeter is an extra fitting parameter in this method. The resulted response times fall into the expected 4–10 seconds range expected for the TA Instrument Nano ITC calorimeter used in this experiment, which confirms the applicability of the method. The kinetics parameters lead to $K_a = k_{on}/k_{off}$ of $4.6 \cdot 10^5 \cdot M^{-1}$, which is close to the obtained value for the reference system of [10]CPP and C_{60}, which suggests little or null cooperativity effect in the interaction of [10]CPP with **P1(C$_{60}$)$_2$**. So the PBI bridge does not seem to have much impact on the complexation with [10]CPP driven by intermolecular concave–convex π–π interactions between the C_{60} substituents of the dumbbell-like molecule and [10]CPP.[7,15,32]

In the last step, NMR titrations were performed in both directions, where a much larger excess of hybrid or [10]CPP could be achieved compared to the ITC experiments. Upon addition of **P1(C$_{60}$)$_2$** to [10]CPP (Exp. A), the singlet of [10]CPP is upfield shifted and steadily broadens with increasing amount of **P1(C$_{60}$)$_2$** (see Figure 7a). Also the signals of the functional hybrid are affected (see Figure S15 in the Supporting Information), first by being downfield shifted in the presence of [10]CPP and then by moving upfield with growing excess of **P1(C$_{60}$)$_2$**, close to the chemical shifts of the pure hybrid without [10]CPP at the end of the titration. Interestingly, the singlet of the OCH_3 groups at 4.00 ppm also becomes increasingly broader at a [10]CPP:**P1(C$_{60}$)$_2$** ratio of 1 : 0.62 and only sharpens again at a ratio of 1 : 3. This broadening indicates coalescence, which is why NMR spectra were recorded at different temperatures (see Figure S2 in the Supporting Information). In the case of the singlet of the PBI protons (8.34 ppm) and the singlet of the OCH_3 groups (4.00 ppm), further peaks appear at low temperatures, as a result from the complexation with [10]CPP. In addition, the [10]CPP signal splits into two peaks, which further confirms the complexation, since the protons pointing to the PBI unit have a different chemical shift than the protons on the other side of the [10]CPP ring pointing towards

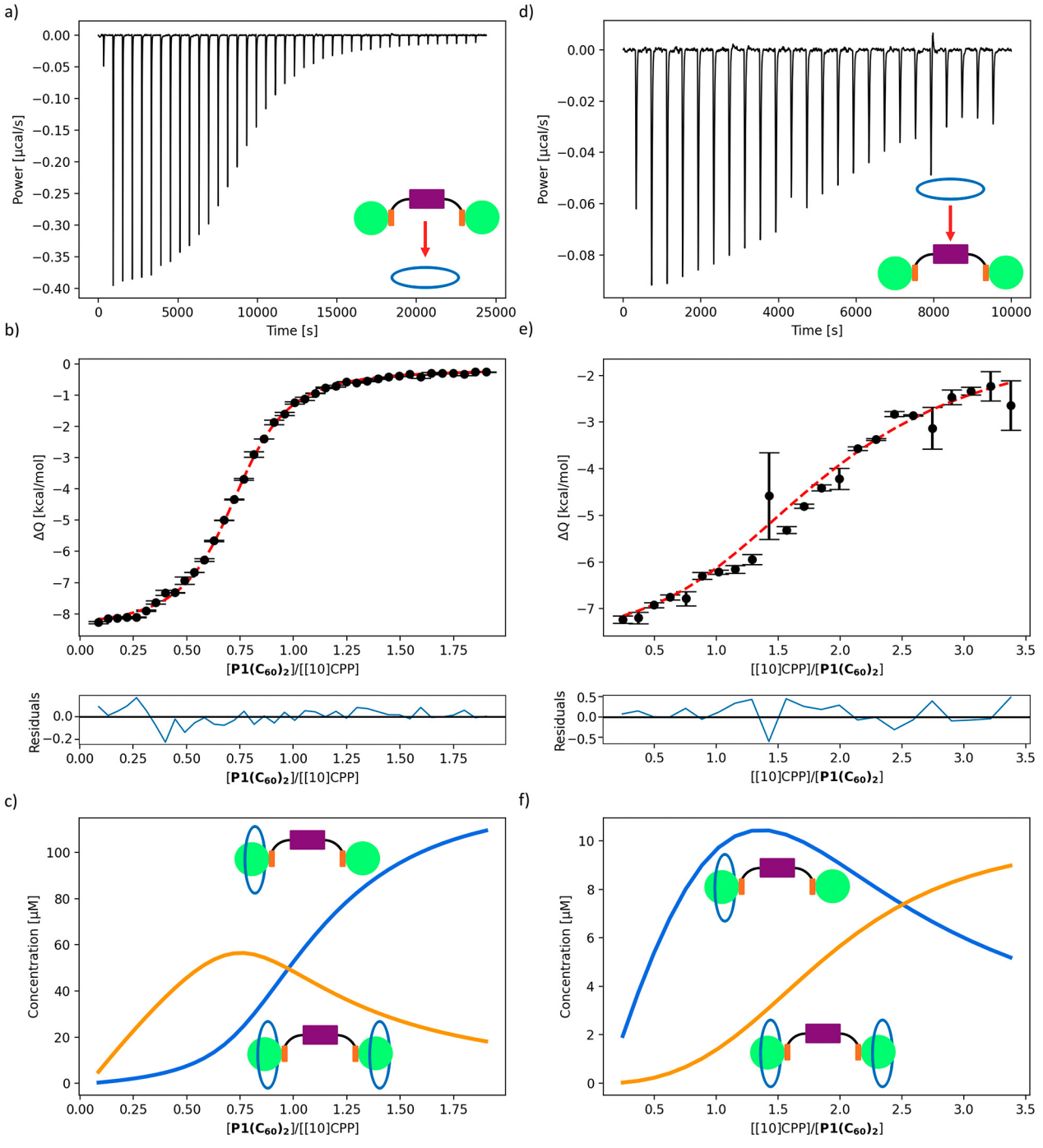

Figure 5 Representative ITC data of the global analysis of the triple titration of **P1(C$_{60}$)$_2$** into [10]CPP (Exp. A) (a–c) together with the triple titration of [10]CPP into **P1(C$_{60}$)$_2$** (Exp. B) (d–f) in *o*-DCB. Experimental thermogram (a, d), the fitting curve (red) using a 2:1 (b) and 1:2 (e) binding model from AFFINImeter software and the experimental data points (black points) as well as residuals of the fit with respect to the experimental data (blue line). Species evolution of [10]CPP⊃**P1(C$_{60}$)$_2$** (blue) and ([10]CPP)$_2$⊃**P1(C$_{60}$)$_2$** (orange) during the titrations (c, f).

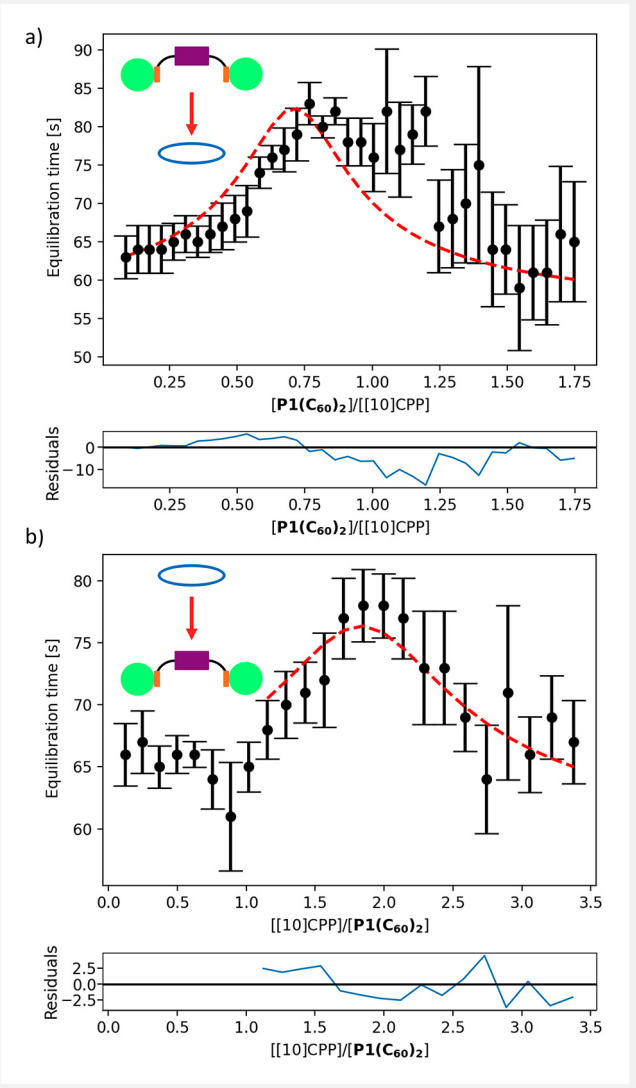

Figure 6 Equilibration time curves for Exp. A (a) and B (b) of **P1(C$_{60}$)$_2$** to calculate the kinetic binding parameters as well as residuals of the fit with respect to the experimental data (blue line).

the exterior side of the molecule.[14] As only two symmetrical peaks can be seen at this stoichiometric proportion, it can be assumed that the hybrid is complexed with [10]CPP either on one side or on both sides but not with two rings on the same side.

Moreover, the splitting of the protons of the alkyl chains at low temperatures is due to the fact that the protons are diastereotopic, since they split at low temperatures even without the addition of [10]CPP. In the inverse experiment (Exp. B), the PBI protons are shifted downfield and changes are again mainly visible in the singlets of the PBI core (see Figure 7b) and the OCH_3 groups (see Figure S16 in the Supporting Information). These first become broader up to a ratio of 1 : 1 and then narrow again. The [10]CPP signal is initially broadened and shifted upfield and then resembles the pure [10]CPP signal more and more in the downfield direction (see Figure S16 in the Supporting Information). When the 1 : 1 mixture is cooled down, the additional peaks at 8.35 and 4.00 ppm are also visible again, as in the previous titration of **P1(C$_{60}$)$_2$** in [10]CPP. The [10]CPP signal also splits, but not symmetrically, since most likely not all the [10]CPP is complexed (see Figure S3 in the Supporting Information). In both titrations, the chemical shifts of the signals from the limiting species were then fitted using the same binding model and the binding constants obtained from the global analysis of the ITC data. In either case, the signals of the molecule where the concentration stayed constant were followed. Thus, when [10]CPP was deficient, the corresponding proton signal at 7.47 ppm was fitted. In the titration with **P1(C$_{60}$)$_2$** as the limiting compound, the signal of the PBI protons at 8.35 ppm was fitted. For both titrations, well-matching fittings could be achieved, which are shown in Figure 7b and 7e. Figure S13 in the Supporting Information shows that the experimental fluorescence data can be also fitted with the same model and same binding constant used in the NMR and ITC analysis. Considering that we were able to perform a multi-technique global fitting of all direct and reverse experiments performed by ITC, NMR and fluorescence using the same binding models, we can forthrightly conclude the formation of 1 : 1 and 2 : 1 [10]CPP-**P1(C$_{60}$)$_2$** complexes, without the presence of 1 : 2 complexes, as shown in Figure 4a.

After the intensive analysis of the complexation of **P1(C$_{60}$)$_2$** with [10]CPP, it was investigated whether the additional PBI unit in **P2(C$_{60}$)$_2$** has a significant influence on the complexation with [10]CPP. NMR titrations with **P2(C$_{60}$)$_2$** and [10]CPP were not possible, since the signals at room temperature are too broad due to the high inversion barrier, which is why the complexation was exclusively investigated with ITC.

When performing the global analysis of the six ITC titration measurements in the same way as it was done for **P1(C$_{60}$)$_2$**, similar binding constants were obtained (see Table 2 and Figure S8 in the Supporting Information): $K_{a,1} = (1.07 \pm 0.02) \cdot 10^6 \cdot M^{-1}$ and $K_{a,2} = (6.2 \pm 0.2) \cdot 10^4 \cdot M^{-1}$. The results agree very well with those of **P1(C$_{60}$)$_2$** with the only difference that for **P2(C$_{60}$)$_2$** the first binding constant $K_{a,1}$ is a bit higher and the second one $K_{a,2}$ a bit lower compared to **P1(C$_{60}$)$_2$**. Consequently, it can be concluded that the complexation with [10]CPP is also possible with the sterically more demanding **P2(C$_{60}$)$_2$** and that the second PBI unit and the rigidity of the system compared to **P1(C$_{60}$)$_2$** have no important influence on the interaction with [10]CPP. In addition, for a mixture of **P2(C$_{60}$)$_2$** and [10]CPP in a molar ratio of 1 : 3, the 1 : 1 complex [10]CPP⊃**P2(C$_{60}$)$_2$** and the 1 : 2 complex ([10]CPP)$_2$⊃**P2(C$_{60}$)$_2$** could also be detected in the gas

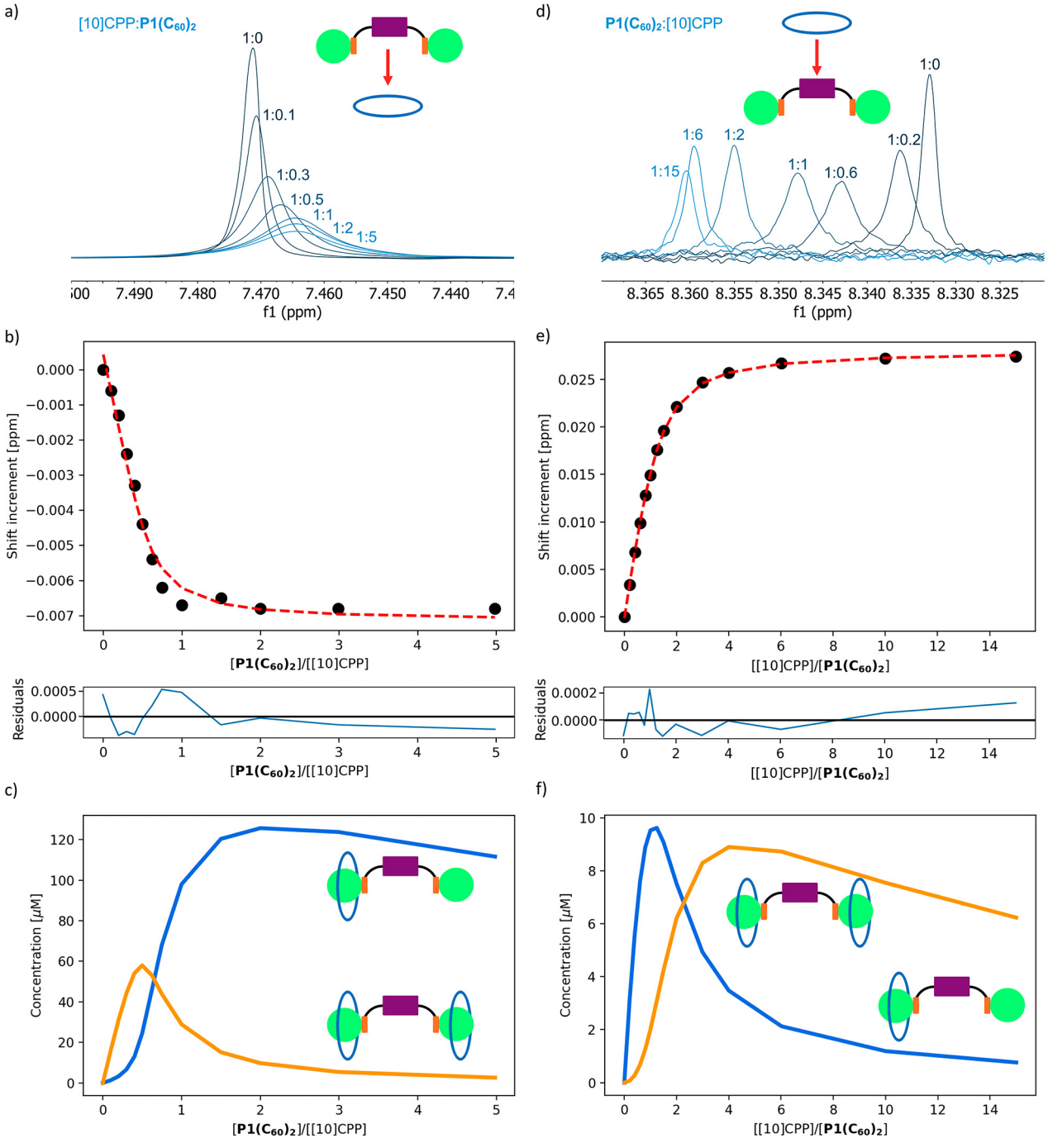

Figure 7 Comparison of the two different NMR titrations of **P1(C$_{60}$)$_2$** into [10]CPP (Exp. A) (a–c) and [10]CPP into **P1(C$_{60}$)$_2$** (Exp. B) (d–f), showing superimposed sections of the ^{1}H NMR spectra of the [10]CPP peak (a) and the PBI protons (d), the fitting curve (red) of the experimental data (black points) using a 2 : 1 (b) and 1 : 2 (e) binding model and binding constants obtained from ITC as well as residuals of the fit with respect to the experimental data (blue line), species evolution of [10]CPP⊃**P1(C$_{60}$)$_2$** (blue) and ([10]CPP)$_2$⊃**P1(C$_{60}$)$_2$** (orange) during the titrations (c, f).

phase, which can be seen in the MALDI-TOF spectrum in Figure S23 in the Supporting Information.

Conclusions

Two dumbbell-like [60]fullerene systems **P1(C_{60})$_2$** and **P2(C_{60})$_2$** have been prepared via a modified *Bingel–Hirsch* cyclopropanation, thus combining the molecular properties of two compound classes. **P2(C_{60})$_2$** with its two PBI units has twice the absorption of **P1(C_{60})$_2$** in *o*-DCB and exhibits strong co-facial π–π stacking. Different-temperature NMR measurements confirm the stacking behavior and show that at −15 °C there is a racemic mixture of (*M*,*M*)-**P2(C_{60})$_2$**/(*P*,*P*)-**P2(C_{60})$_2$** and (*M*,*P*)-**P2(C_{60})$_2$**/(*P*,*M*)-**P2(C_{60})$_2$** in a ratio of approximately 5 : 1 in $C_2D_2Cl_4$. Accordingly, the diastereoselectivity due to the fullerene substituents is lower than that of the precursor molecule **P2** with a ratio of 10 : 1 of the corresponding atropisomers.

In addition, the complex formation of **P1(C_{60})$_2$** and **P2(C_{60})$_2$** with [10]CPP was investigated by spectroscopic and calorimetric techniques in comparison to the reference system [10]CPP⊃C_{60}. It could be concluded that the additional PBI units in dumbbell-like molecules have no significant influence on the complex formation. Global analysis of the ITC titration data was used to detect both the 1 : 1 complex and the 1 : 2 complex with two equivalents of [10]CPP, confirming the formation of the mono- and bis-pseudorotaxanes. In the titrations with addition of the hybrid molecule (Exp. A), the 1 : 1 complex was mainly present at the end, and after the addition of [10]CPP in excess (Exp. B), the 1 : 2 complex was predominantly detected. The bis-pseudorotaxane formation was confirmed also for the more sterically demanding **P2(C_{60})$_2$**, corroborating that the second PBI unit and the rigidity as well as the strong co-facial π–π stacking of the system do not affect the binding with [10]CPP. Furthermore, at the employed stoichiometric ratios, a single [10]CPP bound each fullerene, as evinced by the [10]CPP signal splitting from the NMR studies. Finally, for the first time, the extensive analysis using a multi-technique global fitting of the bis-pseudorotaxane formation from ITC, NMR and fluorescence data allowed getting new insights into the enthalpically driven complexation process, the species distribution, and also the kinetic parameters, which provides important basis for further investigation of fullerene complexes in supramolecular chemistry and may also be of interest for their applications in semiconductor technology and optoelectronics.

Experimental Section

All commercially available chemicals and HPLC solvents were purchased from different chemical suppliers and were used without further purification. The solvents of analytical-reagent grade were purified by distillation with a rotary evaporator. Reaction monitoring was carried out by thin layer chromatography on silica gel 60 F254 0.2 mm on aluminium foil (Merck). For column chromatography, silica gel 60 M (230–400 mesh ASTM, 0.04–0.063 mm) from Macherey-Nagel & Co. KG was used.

Procedures

Synthesis of **P1(C_{60})$_2$**: Under an inert atmosphere, C_{60} (49.0 mg, 68.1 µmol, 5.0 equiv) was dissolved in toluene (15 mL) with the help of an ultrasonic bath and a solution of **P1** (17.7 mg, 13.6 µmol, 1.0 equiv) dissolved in toluene (13 mL) was added. The mixture was stirred at r. t. for 5 min while passing nitrogen through the solution. After addition of I_2 (10.4 mg, 40.9 µmol, 3.0 equiv), the mixture was stirred for another 20 min. A solution of DBU (10.2 µL, 68.1 µmol, 5.0 equiv) in toluene (75 µL) was added dropwise, leading to a colour change from red to dark violet. The mixture was stirred overnight. Diluted HCl (30 mL) was added and the aqueous phase was extracted with toluene (2 × 20 mL). The combined organic phases were dried over $MgSO_4$, filtered and the solvent was removed under reduced pressure. The residue was purified by column chromatography (SiO_2, toluene : CH_2Cl_2 : ethyl acetate 70 : 30 : 0.3 → 0 : 85 : 15, R_f (toluene : ethyl acetate 98 : 2) = 0.23) to obtain **P1(C_{60})$_2$** (18.9 mg, 6.91 µmol, 51 %) as a dark solid. As a side product, the intramolecular isomeric bisadduct (9.12 mg, 4.52 µmol, 33 %) was isolated as a dark violet solid.

IR (ATR): $\tilde{\nu}$ = 2957, 2924, 2866, 1748, 1698, 1662, 1587, 1504, 1285 cm^{-1}.

^{1}H NMR ($CDCl_3$, 400 MHz): δ = 8.20 (s, 4 H, C*H*$_{PBI}$), 7.23–7.16 (m, 8 H, C*H*$_{phenoxy}$), 6.88–6.80 (m, 8 H, C*H*$_{phenoxy}$), 4.80–4.50 (m, 4H, C*H*$_2$), 4.49–4.26 (m, 4 H, C*H*$_2$), 4.02 (s, 6 H, COOC*H*$_3$), 2.35–2.20 (m, 4 H, C*H*$_2$), 1.27 (s, 36H, C*H*$_3$).

^{13}C NMR ($CDCl_3$, 101 MHz): δ = 163.92, 163.73, 163.56 (4C, O–*C*=O and 4C, N–*C*=O), 156.14 (4C, *C*–O), 153.07 (4C, *C*$_{phenoxy}$–O), 147.36 (4C, *C*$_{phenoxy}$), 145.33, 145.32, 145.26, 145.23, 144.96, 144.74, 144.65, 143.91, 143.13, 143.05, 142.95, 142.25, 142.23, 142.01, 141.86, 140.88, 139.51, 138.69 (116C, C_{60}–*sp*^{2}), 133.15 (2C, *C*$_{PBI}$), 126.77 (8C, HC$_{phenoxy}$), 122.25 (4C, *C*$_{PBI}$), 121.01 (4C, *C*$_{PBI}$), 120.26 (4C, *C*$_{PBI}$), 119.73 (2C, *C*$_{PBI}$), 119.54 (8C, HC$_{phenoxy}$), 71.47 (4C, C_{60}–*sp*^{3}), 65.89 (2C, *C*H$_2$), 54.21 (2C, *C*H$_3$), 51.90 (2C, *C*OCCO), 38.31 (2C, *C*H$_2$), 34.49 (4C, *C*(CH$_3$)$_3$), 31.61 (12C, *C*H$_3$), 27.61 (2C, *C*H$_2$).

HRMS (MALDI-TOF, dctb): *m*/*z* calcd for $[C_{198}H_{74}N_2O_{16}]^+$: 2734.5033; found: 2734.4966.

UV-Vis (*o*-DCB): ε (λ_{max}) = 21677 (546), 33677 (588) $M^{-1}\cdot cm^{-1}$ (nm).

Synthesis of **P2(C_{60})$_2$**: C_{60} (47.2 mg, 65.5 µmol, 10.0 equiv) and **P2** (15.3 mg, 6.55 µmol, 1.0 equiv) were dissolved in tol-

uene (30 mL) under an inert atmosphere and sonicated for 10 min, afterwards argon was passed through the solution for 10 min. I_2 (5.49 mg, 21.6 µmol, 3.3 equiv) was added and the mixture was stirred for 15 min. P_1-*t*Bu (5.56 µL, 22.3 µmol, 97% purity, 3.3 equiv) was added and the reaction mixture was stirred overnight at r.t. Most of the solvent was removed under reduced pressure and the residue was purified by column chromatography (toluene/ethyl acetate 98 : 2 → 90 : 10, R_f (toluene : CH_2Cl_2 : ethyl acetate) = 0.31) to yield **P2(C_{60})$_2$** (11.0 mg, 2.92 µmol, 45%) as dark purple solid.

IR (ATR): $\tilde{\nu}$ = 2959, 2924, 2866, 1745, 1699, 1661, 1590, 1505, 1340, 1283, 1268, 1212, 1170 cm^{-1}.

^{1}H NMR ($C_2D_2Cl_4$, 500 MHz, 110 °C): δ = 7.89 (s, 8 H, CH_{PBI}), 7.18–7.13 (m, 16 H, $CH_{phenoxy}$), 6.75–6.68 (m, 16 H, $CH_{phenoxy}$), 4.68–4.40(m, 8 H, CH_2), 4.24–4.06 (m, 8 H, CH_2), 2.20–2.03 (m, 8 H, CH_2), 1.29 (s, 72 H, CH_3).

^{13}C NMR ($C_2D_2Cl_4$, 126 MHz, 110 °C): δ = 163.41 (4C, O–*C*=O), 163.14 (8C, N–*C*=O), 155.85 (8C, *C*–O), 153.36 (8C, $C_{phenoxy}$–O), 147.62 (8C, $C_{phenoxy}$), 145.87, 145.47, 145.46, 145.39, 145.08, 144.94, 144.90, 144.79, 144.09, 143.34, 143.22, 143.20, 142.44, 142.23, 141.14, 139.21 (116C, C_{60}–sp^2), 132.86 (4C, C_{PBI}), 126.58 (16C, $HC_{phenoxy}$), 122.34 (8C, C_{PBI}), 120.71 (8C, C_{PBI}), 120.63(4C, C_{PBI}), 120.24(8C, HC_{PBI}), 119.55 (16C, $HC_{phenoxy}$), 72.52 (4C, C_{60}–sp^3), 65.51 (4C, CH_2), 65.42 (2C, O=CCC=O), 38.30 (4C, CH_2), 34.49 (8C, $C(CH_3)_3$), 31.70 (24C, CH_3), 27.76 (4C, CH_2).

HRMS (MALDI-TOF, dctb): *m*/*z* calcd for $[C_{266}H_{137}N_4O_{24}]^+$: 3769.9617; found: 3769.9589.

UV-Vis (*o*-DCB): ε (λ_{max}) = 47 779 (539), 50 196 (579) $M^{-1} \cdot cm^{-1}$ (nm).

Funding Information

We thank the Deutsche Forschungsgemeinschaft (DFG) for funding this work through SFB 953 "Synthetic Carbon Allotropes" project A9 and the emerging talents initiative (ETI) from FAU to M. E. Pérez-Ojeda.

Acknowledgements

The authors acknowledge Dr. Beatriz Trastoy (Biocruces Bizkaia Instituto Investigación Sanitaria) and Mr. Christian Ortmann (TA Instruments) for their advice on ITC experiments.

Supporting Information

Supporting Information for this article is available online at https://doi.org/10.1055/a-1906-6875.

Conflict of Interest

The authors declare no conflict of interest.

References

(1) (a) Lehn, J.-M. *Chem. Soc. Rev.* **2017**, *46*, 2378. (b) Lu, D.; Huang, Q.; Wang, S.; Wang, J.; Huang, P.; Du, P. *Front. Chem.* **2019**, *7*, 668.
(2) Gokel, G. W.; Leevy, W. M.; Weber, M. E. *Chem. Rev.* **2004**, *104*, 2723.
(3) Rebek, J. J. *Chem. Commun.* **2000**, 637.
(4) Schmidt, B. V. K. J.; Hetzer, M.; Ritter, H.; Barner-Kowollik, C. *Prog. Polym. Sci.* **2014**, *39*, 235.
(5) Yamago, S.; Kayahara, E.; Iwamoto, T. *Chem. Rev.* **2014**, *14*, 84.
(6) Xu, Y.; von Delius, M. *Angew. Chem. Int. Ed.* **2020**, *59*, 559.
(7) Iwamoto, T.; Watanabe, Y.; Sadahiro, T.; Haino, T.; Yamago, S. *Angew. Chem. Int. Ed.* **2011**, *50*, 8342.
(8) Iwamoto, T.; Watanabe, Y.; Takaya, H.; Haino, T.; Yasuda, N.; Yamago, S. *Chem. Eur. J.* **2013**, *19*, 14061.
(9) Ueno, H.; Nishihara, T.; Segawa, Y.; Itami, K. *Angew. Chem. Int. Ed.* **2015**, *54*, 3707.
(10) Rio, J.; Beeck, S.; Rotas, G.; Ahles, S.; Jacquemin, D.; Tagmatarchis, N.; Ewels, C.; Wegner, H. A. *Angew. Chem. Int. Ed.* **2018**, *57*, 6930.
(11) Xu, Y.; Wang, B.; Kaur, R.; Minameyer, M. B.; Bothe, M.; Drewello, T.; Guldi, D. M.; von Delius, M. *Angew. Chem. Int. Ed.* **2018**, *57*, 11549.
(12) Li, K.; Xu, Z.; Deng, H.; Zhou, Z.; Dang, Y.; Sun, Z. *Angew. Chem. Int. Ed.* **2021**, *60*, 7649.
(13) de Juan, A.; Pérez, E. M. *Nanoscale* **2013**, *5*, 7141.
(14) Xu, Y.; Kaur, R.; Wang, B.; Minameyer, M. B.; Gsänger, S.; Meyer, B.; Drewello, T.; Guldi, D. M.; von Delius, M. *J. Am. Chem. Soc.* **2018**, *140*, 13413.
(15) Yuan, K.; Zhou, C.-H.; Zhu, Y.-C.; Zhao, X. *Phys. Chem. Chem. Phys.* **2015**, *17*, 18802.
(16) Hashimoto, S.; Iwamoto, T.; Kurachi, D.; Kayahara, E.; Yamago, S. *ChemPlusChem* **2017**, *82*, 1015.
(17) (a) Werber, L.; Mastai, Y. *Chirality* **2018**, *30*, 619. (b) Brown, A. *Int. J. Mol. Sci.* **2009**, *10*, 3457. (c) Matsuno, T.; Fujita, M.; Fukunaga, K.; Sato, S.; Isobe, H. *Nat. Commun.* **2018**, *9*, 3779.
(18) (a) González-Veloso, I.; Rodríguez-Otero, J.; Cabaleiro-Lago, E. M. *Phys. Chem. Chem. Phys.* **2016**, *18*, 31670. (b) Oleson, A.; Zhu, T.; Dunn, I. S.; Bialas, D.; Bai, Y.; Zhang, W.; Dai, M.; Reichman, D. R.; Tempelaar, R.; Huang, L.; Spano, F. C. *J. Phys. Chem. C* **2019**, *123*, 20567. (c) Shang, X.; Ahn, J.; Lee, J. H.; Kim, J. C.; Ohtsu, H.; Choi, W.; Song, I.; Kwak, S. K.; Oh, J. H. *ACS Appl. Mater. Interfaces* **2021**, *13*, 12278.
(19) (a) Pla, S.; Martín-Gomis, L.; Ohkubo, K.; Fukuzumi, S.; Fernández-Lázaro, F.; Sastre-Santos, Á. *Asian J. Org. Chem.* **2014**, *3*, 185. (b) Baffreau, J.; Ordronneau, L.; Leroy-Lhez, S.; Hudhomme, P. *J. Org. Chem.* **2008**, *73*, 6142. (c) Yuen, J. D.; Pozdin, V. A.; Young, A. T.; Turner, B. L.; Giles, I. D.; Naciri, J.; Trammell, S. A.; Charles, P. T.; Stenger, D. A.; Daniele, M. A. *Dyes Pigm.* **2020**, *174*, 108014.
(20) Spenst, P.; Würthner, F. *J. Photochem. Photobiol. C* **2017**, *31*, 114.
(21) (a) Solymosi, I.; Krishna, S.; Nuin, E.; Maid, H.; Scholz, B.; Guldi, D. M.; Pérez-Ojeda, M. E.; Hirsch, A. *Chem. Sci.* **2021**, *12*, 15491. (b) Pérez-Ojeda, M. E.; Wabra, I.; Böttcher, C.; Hirsch, A. *Chem. Eur. J.* **2018**, *24*, 14088.
(22) (a) Sun, Y.; Li, Z. *Polym. Chem.* **2017**, *8*, 4422. (b) Nuin, E.; Lloret, V.; Amsharov, K.; Hauke, F.; Abellán, G.; Hirsch, A. *Chem. Eur. J.* **2018**, *24*, 4671.

(23) Clark, A. E.; Qin, C.; Li, A. D. Q. *J. Am. Chem. Soc.* **2007**, *129*, 7586.
(24) Baffreau, J.; Perrin, L.; Leroy-Lhez, S.; Hudhomme, P. *Tetrahedron Lett.* **2005**, *46*, 4599.
(25) Ahrens, M. J.; Sinks, L. E.; Rybtchinski, B.; Liu, W.; Jones, B. A.; Giaimo, J. M.; Gusev, A. V.; Goshe, A. J.; Tiede, D. M.; Wasielewski, M. R. *J. Am. Chem. Soc.* **2004**, *126*, 8284.
(26) Hesse, M.; Meier, H.; Zeeh, B., *Spektroskopische Methoden in der organischen Chemie*, Georg Thieme: Verlag, **2005**.
(27) (a) van de Weert, M.; Stella, L. *J. Mol. Struct.* **2011**, *998*, 144. (b) Thordarson, P. *Chem. Soc. Rev.* **2011**, *40*, 1305.
(28) Zhang, X.; Shi, H.; Zhuang, G.; Wang, S.; Wang, J.; Yang, S.; Shao, X.; Du, P. *Angew. Chem. Int. Ed.* **2021**, *60*, 17368.
(29) Piñeiro, Á.; Muñoz, E.; Sabín, J.; Costas, M.; Bastos, M.; Velázquez-Campoy, A.; Garrido, P. F.; Dumas, P.; Ennifar, E.; García-Río, L.; Rial, J.; Pérez, D.; Fraga, P.; Rodríguez, A.; Cotelo, C. *Anal. Biochem.* **2019**, *577*, 117.
(30) Dumas, P.; Ennifar, E.; Da Veiga, C.; Bec, G.; Palau, W.; Di Primo, C.; Piñeiro, A.; Sabin, J.; Muñoz, E.; Rial, J. *Extending ITC to Kinetics with kinITC*. In *Methods in Enzymology, Vol. 567*; Feig, A. L.; Academic Press: Cambridge, **2016**, 157–180.
(31) Muñoz, E.; Sabín, J.; Rial, J.; Pérez, D.; Ennifar, E.; Dumas, P.; Piñeiro, Á. *Thermodynamic and Kinetic Analysis of Isothermal Titration Calorimetry Experiments by Using KinITC in AFFINImeter*. In *Microcalorimetry of Biological Molecules: Methods in Molecular Biology, Vol. 1964;* Ennifar E.; Humana Press: New York, NY, **2019**, 225–239.
(32) Kawase, T.; Kurata, H. *Chem. Rev.* **2006**, *106*, 5250.